

Io's Volcanic and Sublimation Atmospheres

MIGUEL A. MORENO

Evalcomp Corporation, Los Angeles, California 90025

GERALD SCHUBERT

Institute of Geophysics and Planetary Physics and Department of Earth and Space Sciences, University of California, Los Angeles, California 90024-1567

JOHN BAUMGARDNER

Los Alamos National Laboratory, Los Alamos, New Mexico 87545

MARGARET G. KIVELSON

Institute of Geophysics and Planetary Physics and Department of Earth and Space Sciences, University of California, Los Angeles, California 90024-1567

AND

DAVID A. PAIGE

Department of Earth and Space Sciences, University of California, Los Angeles, California 90024-1567

Received June 16, 1988; revised May 31, 1991

Computer simulations of SO₂ and H₂S frost sublimation and SO₂ day and nightside volcanic atmospheres on Io are presented. The models include a surface temperature which is a function of distance from the volcanic vent or subsolar point, sublimation and condensation with a sticking coefficient of unity, and a crude radiative transfer approximation. The full three-dimensional, axisymmetric gas dynamic equations are solved numerically using a time explicit, finite volume formulation. Neither a SO₂ frost sublimation atmosphere nor a SO₂ Pele-type eruption centered on the dayside extends into the nightside. However, if the volcanic emissions contain a gas with a lower condensation rate than SO₂, for example H₂S, then a Pele-type volcanic eruption centered on the dayside can reach the terminator with the pressure required by the Pioneer 10 radio occultation measurements. Also, the atmosphere generated by a SO₂ Pele-type volcano located at a distance of ~400 km from the terminator can extend to the terminator with the required Pioneer 10 radio occultation pressure. An extended nightside atmosphere could be formed by horizontal flow from multiple volcanoes located on the nightside. Both sublimation and volcanic atmospheres produce horizontal supersonic winds away from the subsolar point or the volcanic vent. The sublimation atmosphere is driven mainly by horizontal pressure gradients determined by surface temperatures. The volcanic atmosphere is driven by pressure gradients determined by the source rate. The near surface momentum flux for a dayside Pele-type volcanic atmosphere is consistent with observations of winds blowing vent emis-

sions at 700 km from the main vent. The volcanic atmosphere features a shock that forms as the gas falls supersonically toward Io's surface. The volcanic nightside shock comes closer to Io's surface than the dayside shock. No shock develops in the sublimation atmosphere. Sublimation and condensation produce patterns of surface deposits which are characteristic of the two types of atmospheres. A sublimation atmosphere develops a resurfacing band pattern. Sublimation removes mass from an equatorial band of $\sim \pm 27^\circ$ of Iographic latitude, while condensation deposits mass poleward of $\pm 27^\circ$ latitude. The maximum condensation rate per Io rotation period occurs at $\sim 50^\circ$ Iographic latitude and the rate decays to zero at $\sim 80^\circ$ latitude. Volcanic atmospheres have condensation deposits in the form of rings that fall within the particulate plume and are caused by plume shock conditions. The volcanic model is quantitatively consistent with Voyager observations of ring deposits. Volcanic eruptions expose SO₂ and other possible gaseous constituents of the plume such as sodium to sputtering by corotating torus ions in times very short (~1 hr) compared to diffusion and dissociation times. Thus, the source of neutrals to the Jovian magnetosphere reflects the volcanic source composition and meets the constraints imposed by multiple torus observations, particularly the ratio of oxygen to sulfur. Furthermore, the elevation of the exobase above the surface in the vicinity of volcanic vents may locally increase the neutral sputtering rate if the diversion of magnetospheric plasma flow around Io is considered. © 1991 Academic Press, Inc.

1. INTRODUCTION

Ingersoll *et al.* (1985), hereafter IN85, considered the supersonic meteorology of Io using vertically integrated equations in which the mass, energy, and horizontal momentum of atmospheric columns are functions only of horizontal distance from the subsolar point. They considered flows driven by sublimation of SO₂ frost, the vapor pressure of which was assumed to vary by orders of magnitude from dayside to nightside. Here we present a model of the sublimation atmosphere and a model of a volcanic atmosphere by employing a numerical gas dynamic representation in which flow variables are functions of both altitude and horizontal distance from the source and attempt to reconcile the results with observations of Pioneer 10, Voyager 1, and the IUE spacecraft. Most previous models of Io's atmosphere have encountered some differences with observations. For example, Pioneer 10 radio occultation data suggest that the atmospheric pressure at the terminator is 10⁻⁴ Pa (Kliore *et al.* 1975), whereas SO₂ surface frost equilibrium and dynamic models predict a pressure from 10 to 100 times smaller (IN85). IN85 used their model to test the hypothesis that hydrodynamic flow could carry sufficient SO₂ to the terminator to explain the Pioneer 10 occultation measurement. They rejected the hypothesis and speculated that another gas such as O₂ might be present on the nightside.

Ground-based observations of the thermal behavior of Io's surface after it emerges from Jupiter's shadow indicate that it has a porosity of about 65% (Simonelli and Veverka 1986). These authors infer a surface pressure at the subsolar point of 10⁻⁷ Pa by assuming SO₂ equilibrium with buried condensate. On the other hand, SO₂ frost exposed on the surface can reach temperatures of 120–125 K at the subsolar point (McEwen *et al.* 1988, Ingersoll 1989), implying saturation vapor pressures of 10⁻³ to 10⁻² Pa. The SO₂ hydrodynamic model (IN85) shows that atmospheric pressures are only a few percent lower than the saturation vapor pressures, and therefore could be in the range 10⁻³ to 10⁻² Pa.

Voyager 1, ground-based, and rocket observations of the hot Io torus imply that the neutral source ratio of oxygen to sulfur is between 1:3 (Moreno *et al.* 1985) and 2:1 (Shemansky and Smith 1981; Shemansky 1987; Barbosa and Moreno 1987). However, the SO₂ surface frost equilibrium model predicts a ratio of up to 10:1 (Summers 1985) because the sublimed gas remains in the atmosphere long enough for photodissociation and separative diffusion to take place. A way out of this problem may be found in the model of Hunten (1985), in which the diffusion equations for two components with mutual drag terms are considered. It is found that the lighter components (O) may drag the heavier (SO₂, S₂) components with a tendency to equalize their scale heights, and thus the O:S ratio may approach 2. The model, however, is not

intended to simultaneously address other problems such as the near-surface pressure at the terminator, for which all models so far predict a value much lower than that required by observations.

Accordingly, we consider it worthwhile to propose and evaluate an entirely different type of atmosphere. Moreno *et al.* (1986) first introduced the concept and a model of a volcanic atmosphere of Io in an effort to reconcile Voyager and Pioneer observations. The work presented here is an extension of that effort. In Moreno *et al.* (1986) large volcanic plumes serve as the source of the atmosphere (see also a recent study of Io volcanic atmospheres by Ingersoll (1989)).

The abundant volcanic activity on Io observed by Voyagers 1 and 2 (Strom *et al.* 1979, McEwen and Soderblom 1983), the estimates of comparable gas to solid mass ejection rates for the volcanic plumes (Collins 1981), and the estimates of large volcanic resurfacing rates (Johnson *et al.* 1979) strongly suggest that gases such as SO₂, S₂, and H₂S emitted in volcanic plumes expand to form a transient atmosphere, strongly localized around centers of volcanic activity. IUE (International Ultraviolet Explorer) measurements indicate an average disk pressure of 10⁻⁴ Pa (Butterworth *et al.* 1980), while the Voyager IRIS (Infrared Spectrometer) experiment (Pearl *et al.* 1979) measured a pressure of 10⁻² Pa in the region of the Loki volcano located on the Jupiter-facing quadrant of the trailing hemisphere. Also, as demonstrated in Moreno and Barbosa (1986), cold torus plasma conditions, i.e., molecular ion composition, mass, and energy balance, are consistent with the presence of a neutral SO₂ cloud in the cold torus region. This suggests that the observed volcanic plumes may serve as a significant source for Io's atmosphere.

In the following, we first describe more completely the observations that we view as critical tests of an atmospheric model and we summarize features of previous atmospheric models that do not accord with observations. Our numerical gas dynamic model is introduced next. In order to validate our numerical approach, we first simulate a sublimation atmosphere with radiative emissivity $\epsilon = 0$ studied by IN85. For the purpose of comparison we use the assumed surface temperature of IN85, and discuss the similarities and differences between their solution and ours. We introduce a crude model of radiative heat transfer and assess its importance. We then describe the results of a simulation of an atmosphere generated by a volcanic eruption and show how such an atmosphere differs from a sublimation atmosphere. Finally, we compare our model of Io's volcanically controlled atmosphere with observations to demonstrate generally satisfactory agreement.

2. OBSERVATIONS

The first indirect evidence for an atmosphere on Io was the photometric measurement of Io's post-eclipse bright-

ening (Binder and Cruikshank 1964). These observations suggested the existence of a frost or snow deposit or haze layer caused by low temperatures during eclipse. However, during the two Voyager encounters three eclipse reappearances were observed and there was no whole disk brightening at the 10% level (Summers 1985). Indeed, the earlier observations have been questioned (N. Schneider, personal communication, 1989). Alternatively, post-eclipse brightening may be sporadic, an unpredictable phenomenon perhaps related to large variability in atmospheric density.

Spectroscopic observations of the occultation of β -Scorpii C by Io (Smith and Smith 1972) placed an upper limit of 10^{-2} Pa on the surface pressure of an Io atmosphere for assumed isothermal conditions and a surface temperature of 100 K. Radio occultation measurements by Pioneer 10 (Kliore *et al.* 1975) detected an ionosphere on Io and suggested the presence of a supporting atmosphere with a surface pressure of 10^{-3} Pa to 10^{-4} Pa at the terminator (Kliore *et al.* 1975).

The Voyager 1 IRIS experiment detected the $\nu_3 = 1350$ cm^{-1} absorption band of SO_2 in the region centered on the active volcano Loki (Pearl *et al.* 1979). The measured SO_2 abundance was attributed to a localized atmosphere with a surface pressure of 1.4×10^{-2} Pa.

Studies of the thermal response of Io's surface as it emerges from the shadow of Jupiter (Matson and Nash 1983) suggest that the surface may be very porous, i.e., $\sim 85\%$. This conclusion is supported by the more recent eclipse observations of Simonelli and Veverka (1986) who conclude that the surface of Io has a porosity of 65%. Matson and Nash (1983) theorize that low porosity implies subsurface cold traps that limit the surface pressure to 10^{-7} Pa.

IUE observations of Io in the spectral range of 2900 to 3100 \AA suggest a disk average surface pressure of 10^{-4} Pa (Butterworth *et al.* 1980). However, these results may represent an underestimate of the SO_2 abundance (Belton 1982). More recent observations (Lellouch *et al.* 1990) detected SO_2 gas at pressures as high as 3×10^{-3} Pa.

Recent observations (Schneider *et al.* 1987) reveal that Io has a global sodium atmosphere and suggest a globally thin atmosphere of heavier constituents by extrapolation of the relative source rates of neutrals for the hot torus and for the Io-related sodium cloud.

Indirect evidence for atmospheric structure comes from examination of vapor streams emitted from small vents roughly 700 km from Pele. Voyager observations show that these markings extend up to 70 km in a direction radially away from the source of the Pele volcanic eruption. These features have been explained as local venting of particles into a horizontal flow away from Pele with a source rate ranging from 10^4 to 10^6 kg/sec, pressures of 10^{-2} Pa, and wind velocities of 130 m/sec (Lee and Thomas 1980). The gas densities and velocities necessary

to suspend and transport 0.1- to 10- μm particles at such distances are consistent with a locally thick atmosphere of volcanic origin flowing radially away from the source.

Voyager 2 detected nine active plumes on Io and Voyager 1 detected eight active plumes four months later. The heights of the plumes varied between 100 and 300 km and their widths between 100 and 1400 km, with ejection velocities at the vents varying between 0.5 and 1.0 km/sec (Strom and Schneider 1982). These observations, together with the IRIS detection of SO_2 in the Loki region with a pressure of 1.4×10^{-2} Pa, suggest that large amounts of volatiles are injected in the immediate vicinity of the surface of Io.

Studies of multicolor Voyager images of the Loki plume by Collins (1981) reveal that the plume is mostly composed of two populations of particles and SO_2 gas. The first population consists of particles with radii 0.001 to 0.01 μm and total mass of 10^8 to 10^{11} kg, while the second population consists of particles with radii ≥ 1.0 μm and a much smaller total mass of 10^5 kg. The spectroscopically identified sulfur dioxide gas (IRIS experiment; Pearl *et al.* 1979) contributes a mass of 2×10^8 kg to the plume. The plume is thus composed of sulfur dioxide gas and very fine particles in roughly equal amounts by mass.

These observations of volcanic gases could be consistent with the IUE measurements indicating a globally thin atmosphere (i.e., a disk-averaged pressure of 10^{-4} Pa) if volcanic gases build locally thick atmospheres near volcanoes that evolve into thin atmospheres at large distances from the vents. Since most of the volcanoes are located near the equatorial region (McEwen and Soderblom 1983), this view is also consistent with the observed lack of polar caps of condensed sulfur dioxide. Plume depositional rates necessary to explain the observed absence of craters on the surface of Io are about 0.1 cm/year to 4×10^{-4} cm/year as a lower limit (Johnson *et al.* 1979). This implies plume source rates of 10^4 to 10^6 kg/sec averaged over a few hundred thousand years.

3. PREVIOUS MODELS OF THE ATMOSPHERE OF IO AND OF PROPERTIES OF VOLCANIC PLUMES

Most models of the atmosphere of Io have been based on the assumption of equilibrium with a surface SO_2 frost at a constant temperature of 130 K or at a temperature consistent with radiative equilibrium with the solar flux, $T_s = [80(\cos \theta)^{1/4} + 50]$ K for $\theta < 90^\circ$, and $T_s = 50$ K for $\theta > 90^\circ$, where θ is the angle from the subsolar point. In a number of models, the upper atmosphere is static with a composition established by dissociation of sulfur dioxide by solar UV and the diffusive separation of oxygen and sulfur (Kumar 1984, Summers 1985). IN85 have presented a hydrodynamic model in which sulfur dioxide sublimates from the subsolar hemisphere with a local subsolar point surface pressure of 10^{-2} Pa, expands at supersonic speeds

toward the nightside, and condenses away from the source. They have also considered a range of subsolar surface temperatures from 110 to 130 K and discussed how the problem would scale to any vapor pressure. The assumption that the atmospheric gas is in equilibrium with a surface sulfur dioxide frost at 130 K or at 110 K at the subsolar point is itself controversial. As previously noted, the measurements of Simonelli and Veverka (1986) suggest that the surface of Io has at least 65% porosity. In the absence of surface frost deposits, the atmosphere would be in equilibrium with a substrate much colder than the uppermost surface of Io, suggesting a much lower surface atmospheric pressure than used in surface frost sublimation models. For a highly porous surface the temperature at the subsolar point is 130 K while at only one centimeter below the surface, the temperature is 100 K (Matson and Nash 1983).

A serious shortcoming of models with a relatively static structure is that they predict an exospheric oxygen abundance of about 10 relative to sulfur. This ratio is inconsistent with the observed torus ion composition, although as noted above, atmospheric drag (Hunten 1985) may serve to modify these predicted relative abundances. The IN85 model has the difficulty that it predicts significant condensation in the polar regions. Voyager observations indicate that there are no visible, bright, polar caps on Io. This feature was discussed by IN85.

Published models of volcanic plumes on Io have been mostly qualitative and based on analysis of ballistic trajectories and a simple aerodynamic model (Cook *et al.* 1979). The essential difficulty of the ballistic models is that they predict plume shapes which clearly disagree with observations, particularly at the outer edges near the surface, as acknowledged by the authors (Cook *et al.* 1979). The shock disk or simple aerodynamic models based on ballistic trajectories and shock dynamic arguments do not predict any atmosphere beyond the plume region (Cook *et al.* 1979). From Voyager observations (Strom *et al.* 1979) it is known that there are surface deposits in the form of rings inside the volcanic plumes, which should be explained by volcanic plume models. Neither the aerodynamic models nor the ballistic models of volcanic plumes account for the ring deposits (Strom *et al.* 1979). Furthermore the models do not explain the observed filamentary structure in the upper regions of the plume nor the abrupt horizontal ends of these structures observed by Voyager 1 (Collins 1981).

This brief critique of models of the atmosphere and the plumes reveals a number of problems and suggests the need for a major reconsideration of the models. It was on this basis that Moreno *et al.* (1986, 1987) developed the concept of a volcanic atmosphere and carried out numerical simulations of volcanic atmospheres to address the major issues. These volcanic atmosphere simulations re-

vealed that there is substantial horizontal flow away from the plume and that, under certain surface condensation conditions, a spatially extended atmosphere can be formed, i.e., one which is several plume diameters in width. More recently, Ingersoll (1989) has developed a simplified analytical model for a volcanic atmosphere. In this paper we present the first detailed description of the numerical gas dynamic model of volcanic atmospheres (Moreno *et al.* 1986, 1987).

4. NUMERICAL GAS DYNAMIC MODELS OF ATMOSPHERES

The numerical models we develop are based on the equations of inviscid, compressible gas dynamics:

$$\frac{\partial \rho}{\partial t} + \nabla \cdot [\rho \mathbf{u}] = 0 \quad \text{Mass conservation} \quad (1)$$

$$\frac{\partial [\rho \mathbf{u}]}{\partial t} + \nabla \cdot [\rho \mathbf{u} \mathbf{u}] = -\nabla p + \rho \mathbf{g} \quad \text{Momentum conservation} \quad (2)$$

$$\frac{\partial [\rho E]}{\partial t} + \nabla \cdot [\rho E \mathbf{u}] = -p \nabla \cdot \mathbf{u} + \frac{g \rho \epsilon \sigma}{p_0} [T_s^4 - T^4] \quad \text{Energy conservation} \quad (3)$$

$$p = \rho [k/M_{\text{SO}_2}] T \quad \text{Equation of state} \quad (4)$$

In Eqs. [1]–[4], ρ is the mass density, \mathbf{u} is the velocity, \mathbf{g} is Io's acceleration of gravity which is expressed as a function of height, p_0 is a reference atmospheric surface pressure, E is the specific internal energy, T_s is the surface temperature, which is specified as a boundary condition, T is the atmospheric temperature, p_s is the surface atmospheric pressure, σ is the Stefan–Boltzmann constant, k is the Boltzmann constant, M_{SO_2} is the mass of the SO_2 molecule [1.1×10^{-25} kg], and ϵ is the atmospheric emissivity.

The final term in the energy equation [3] represents a crude attempt to incorporate effects of radiative transfer in a dynamical model of a sublimation or volcanic atmosphere. The term accounts for the radiative cooling of each mass element of the atmosphere to space and for the radiative heating of each atmospheric element by thermal emission from the surface, which is assumed to be a blackbody at temperature T_s . There are several indications that radiative transfer plays a role in determining the structure and dynamics of Io's atmosphere. The photoionization of SO_2 gas by solar ultraviolet radiation causes significant heating on the day side (Kumar 1980; Kumar and Hunten 1982). Infrared emission by SO_2 in the ν_1 (1100–1200 cm^{-1}), ν_2 (480–560 cm^{-1}), and ν_3 (1320–1390 cm^{-1}) bands

can result in atmospheric cooling on both the day and the night sides (Kumar 1985). Solid particles ejected from volcanoes and H_2S gas should also be optically active at solar and infrared wavelengths.

The emissivity of an SO_2 atmosphere on Io is estimated in Appendix A, which also provides additional discussion of the limitations of our simplified radiation treatment. We find that the emissivity of an SO_2 atmosphere may be as large as 10^{-5} , a value consistent with the Voyager IRIS observations (Pearl *et al.* 1979) of the Loki region. In the following calculations we consider the effects of radiative transfer for emissivity values varying from 0 to 10^{-5} . For $\epsilon = 10^{-5}$, the time scale for radiative cooling of the atmosphere is of the order of an hour, while the time scale for the formation of the atmosphere by horizontal flow is several hours (~ 5 h). This latter estimate is a lower limit obtained by use of the speed of sound at the subsolar point surface temperature of 130 K. Therefore, we can anticipate that radiation will influence the atmospheric structure and dynamics for ϵ as large as 10^{-5} . In evaluating the radiation term in the energy equation, a value of $p_0 = 5 \times 10^{-5}$ Pa is used.

Our model also includes surface condensation and sublimation at the rate \dot{m} [mass/area/time]:

$$\dot{m} = [(\alpha M_{SO_2} v_s)/(kT_s(2\pi)^{0.5})] \times [p_v - p_s], \quad (5)$$

where v_s is the thermal velocity at the surface temperature T_s and p_v is the vapor pressure corresponding to the surface temperature T_s . Here v_s is $[3kT_s/M_{SO_2}]^{1/2}$ and α is the sticking coefficient, a measure of the affinity of the surface to incident sulfur dioxide molecules. The value of the sticking coefficient is taken to be 1 for both the sublimation and the volcanic atmospheres. The value of 1 is chosen for consistency with some laboratory measurements (Bryson *et al.* 1974) which show that for the range of temperatures on Io α is >0.5 . Since the surface properties of Io have not been well reproduced in the laboratory, the sticking coefficient is uncertain. In addition, we use

$$p_v = A \exp[-B/T_s], \quad (6)$$

where $A = 1.52 \times 10^{13}$ Pa and $B = 4510$ K.

If $p_s > p_v$ then condensation occurs, while if $p_v > p_s$ sublimation takes place. The sublimed mass element carries with it the thermal energy corresponding to the local surface temperature, but carries no momentum. In the condensation region the condensed mass element carries with it, to the surface, its thermal energy and momentum. Latent heat of condensation is not included in the model since it is assumed to be deposited into the planet's surface rather than into the atmosphere (D. M. Hunten, personal communication 1988). No frictional drag is included in our present model. However, this feature will be added

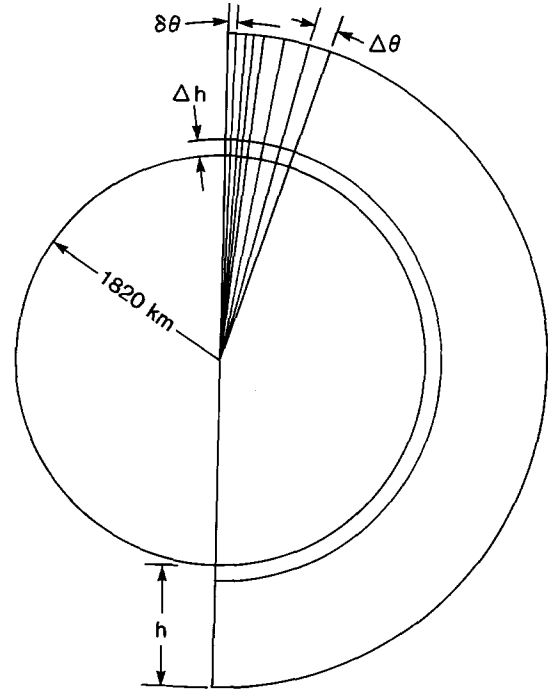


FIG. 1. Computational grid for the numerical simulations. For the sublimation atmosphere the grid consists of cells of constant width $\delta\theta = \Delta\theta = 0.023$ rad (where θ is the polar angle relative to the subsolar axis) and constant height $\Delta h = 0.8$ km. The grid extends from the surface to an altitude $h = 40$ km and from $\theta = 0$ to $\theta = 180^\circ$. For the volcanic atmosphere, the grid consists of cells of height $\Delta h = 5$ km. The cells have variable width. There are four cells assigned to the vent region with $\delta\theta = 0.001$ rad. The cell width then increases smoothly over the next 16 cells to a maximum width of $\Delta\theta = 0.025$ rad. The grid extends from the surface to $h = 800$ km and from $\theta = 0$ to 180° . Rotational symmetry about the polar axis is assumed.

in future improvements of the model, since it could be significant for the horizontal velocity and atmospheric properties near the surface (D. M. Hunten, personal communication 1988).

The gas dynamic equations are numerically integrated in a spherical shell geometry that includes an axis of cylindrical symmetry passing through either the subsolar point or the location of a volcanic plume. Boundary conditions and model parameters are discussed in the next section and the numerical method is described in Appendix B.

5. MODEL PARAMETERS AND BOUNDARY CONDITIONS

We have carried out seven simulations, four for SO_2 sublimation atmospheres, one for a sublimation H_2S atmosphere, and two for volcanic SO_2 atmospheres. The spatial domain (Fig. 1) consists of a spherical shell with thickness $h \gg$ scale height H ($h = 40$ km for the sublimation atmospheres and 800 km for the volcanic atmospheres). The grid is uniform for the sublimation atmospheres. The

width of each cell $\Delta\theta$ is 1° and the height Δh is 0.8 km. The grid for the volcanic atmospheres is nonuniform; four cells are assigned to the vent region with a width $\delta\theta = 0.001$ rad. The cell width increases smoothly over the next 16 cells up to a constant width of $\Delta\theta = 1^\circ$. The cell height Δh is 5 km with the first cell centered at 2.5 km above the surface. The variable grid increases the resolution of the simulations and provides a better model of the behavior of the gas near the volcanic vent. It also ensures the stability of the code by reducing the change of pressure and velocity across cell boundaries in the region of large gradients.

For the sublimation atmosphere the radial velocity at the surface in the sublimation region is zero. For the volcanic atmospheres we choose the radial velocities at the source (the vent) as follows. For the first cell near the axis of the vent we use an exit speed of 1 km/sec. For the second cell we take an exit speed of 900 m/sec; we use 600 and 200 m/sec for the third and fourth cells, respectively. This is consistent with studies of volcanic plumes (Strom and Schneider 1982, Kieffer 1982), which show that the maximum velocity of the gas as it exits the vent is 1 km/sec. The total source rate is taken to be 10^6 kg/sec as indicated by resurfacing arguments (Johnson *et al.* 1979).

For the sublimation atmosphere simulations and for the dayside volcanic atmosphere simulation, the model surface is kept at a temperature $T_s(\theta)$ [IN85] prescribed as:

$$\begin{aligned} T_s(\theta) &= [80(\cos \theta)^{1/4} + 50] \text{ K} && \text{for } \theta < 90^\circ \\ &= 50 \text{ K} && \text{for } \theta > 90^\circ, \end{aligned} \quad (7)$$

where θ is the angle from the subsolar point. This choice of surface temperature allows us to compare our results directly with those of IN85. However, for the simulation of a nightside volcanic atmosphere, we use a constant surface temperature of 90 K. We prefer to use 90 K in the nightside because it is in better accord with observations (Johnson and Matson 1989). In both sublimation and volcanic atmospheres, surface to atmosphere conductive heat transport contributes in a minor way to determining T_s .

In addition to the previously noted cylindrical symmetry axis, the boundary conditions for both sublimation and volcanic atmospheres include an outer boundary where outflow but no inflow is allowed. At time $t = 0$, in both the sublimation atmosphere and the volcanic atmosphere, the background atmosphere is isothermal with a temperature of 50 K and a constant pressure equal to the vapor pressure of SO_2 at a temperature of 50 K.

In both atmospheres, sublimation and volcanic, the horizontal velocity is set to zero along the symmetry axis.

Where the symmetry axis intersects the surface a volcanic source strength may be specified. To model a sublimation atmosphere, we assume no sources other than surface sublimation with strength determined by the ratio of local near-surface atmospheric pressure to surface vapor pressure.

The first model we consider is that of a sublimation atmosphere where the surface temperature T_s is determined by radiative equilibrium between solar irradiation and radiative emissions from the surface, as in Eq. (7), and $\varepsilon = 0$. We then simulate a sublimation atmosphere with $\varepsilon = 10^{-5}$, 10^{-6} , 10^{-7} and the same boundary conditions as for the $\varepsilon = 0$ case. By comparing the simulations with nonzero emissivity and $\varepsilon = 0$, we can estimate the effects of atmospheric radiative transfer on atmospheric properties such as pressure, temperature, and horizontal velocity. We also compare our $\varepsilon = 0$ results with those of IN85.

We next simulate the atmosphere generated by a large volcanic source and include radiative heat transfer by using $\varepsilon = 10^{-5}$. We center the volcanic source at the subsolar point and allow SO_2 gas to expand from a surface vent and flow out into a thin, spherical shell, isothermal background atmosphere with a temperature of 50 K. The properties of the background atmosphere are suggested by the studies of the thermal behavior of Io's surface after emergence from eclipse (Simonelli and Veverka 1986). The ejected SO_2 gas is assumed to be ideal with $\gamma = 1.33$ and $c_p = 520$ J/kg K, where c_p is the specific heat at constant pressure and γ is the ratio of c_p to specific heat at constant volume.

We take the exit temperature as 100 K from studies of the thermodynamics of volcanic eruptions and overpressure plumes (Kieffer 1982). According to observations by the Voyager spacecraft (Strom and Schneider 1982), the vent of Pele is 8 km in width and 24 km in length. For simplicity, we assume a circular vent with approximately the same area as that of the observed vent (radius = 8.38 km). The source rate we use, 10^6 kg/sec, is in the range proposed by Lee and Thomas (1980) from analysis of surface gas flow from the Pele region. The Johnson *et al.* (1979) requirement of a particulate source strength of 10^4 to 10^6 kg/sec on average over a few hundred thousand years and the 1 : 1 ratio of gas to particulates in the plumes suggest a gas source rate of 10^4 to 10^6 kg/sec, so our assumed volcano is a large one.

In the model for the volcano, the source is turned on at time $t = 0$ and eruption continues over the entire interval of the simulation, $t = 3 \times 10^4$ sec. The choice of this simulation time scale is based on a comparison of the results at $t = 3 \times 10^4$ sec with those of previous time steps (e.g., 2.0×10^4 sec). This comparison reveals that the system has reached a steady state.

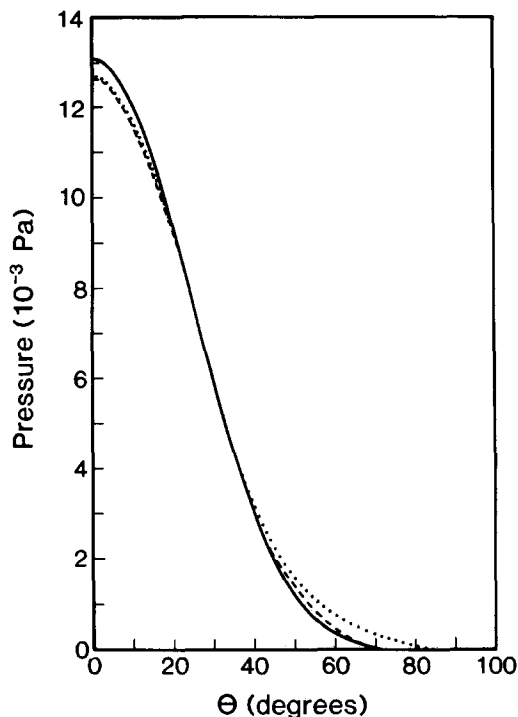


FIG. 2. Near surface pressure at $z = 0.4$ km (dashed curve), surface pressure from the IN85 model (dotted curve), and surface vapor pressure (solid curve) are plotted as functions of θ for the sublimation atmosphere with $\varepsilon = 0$. The source region, i.e., the region where sublimation takes place, extends from the subsolar point to $\theta = 37^\circ$.

6. SUBLIMATION ATMOSPHERE

6.1. Test of the Model with Zero Atmospheric Emissivity

In order to check the code's performance, we ran it for conditions similar to those of the IN85 model and compared our results with the results of IN85. In what follows we describe the comparison.

The IN85 model set the atmospheric emissivity $\varepsilon = 0$, prescribed the surface temperature $T_s(\theta)$, as given by Eq. (7), and used vertically integrated forms of the horizontal momentum equation and the energy equation to determine height-averaged properties of the atmosphere. The one-dimensional constraint on the IN85 model atmosphere prevents the gas from expanding and cooling at the subsolar point. In our numerical simulation, the gas is allowed to expand and cool everywhere, including the subsolar point. Both the IN85 model and our numerical model regard the surface either as a source or a sink of SO_2 . In the source region, the vapor pressure exceeds the atmospheric pressure and in the sink region the converse is true.

Figure 2 shows the near surface (height $z = 0.4$ km)

atmospheric pressure for our model and the surface pressure for the IN85 model as functions of angular distance θ from the subsolar point. There is good agreement between the models, especially over the sublimation region $\theta \leq 37^\circ$. Both models agree on the location and extent of the source (sublimation) and sink (condensation) regions. The source region extends from the subsolar point to $\theta = 37^\circ$, i.e., to where the atmospheric pressure becomes higher than the vapor pressure of SO_2 at the surface temperature ($p_v(\theta)$ is also shown in Fig. 2). The sink or condensation region extends beyond $\theta = 37^\circ$. However, at $\theta = 80^\circ$, the mean free path for collisions between SO_2 molecules in the atmosphere exceeds the scale height (based on $T_s(\theta)$), and the fluid model does not rigorously apply beyond $\theta = 80^\circ$. For $\theta > 80^\circ$, the SO_2 molecules are expected to hop a few scale heights and stick to the surface. Expansion in the numerical model causes a decrease in atmospheric pressure with height at the subsolar point and elsewhere as compared to the pressure in the lowest cell centered at $z = 0.4$ km and plotted in Fig. 2.

Near surface atmospheric temperature at altitudes $z = 0.4$, 2, and 10 km in our numerical model, the vertically averaged atmospheric temperature in the IN85 model, and the surface temperature $T_s(\theta)$ are plotted versus θ in Fig. 3. As a consequence of expansion at the subsolar point, the temperature at $\theta = 0^\circ$ drops by about 5 K between the surface and altitude $z = 2$ km in the numerical model.

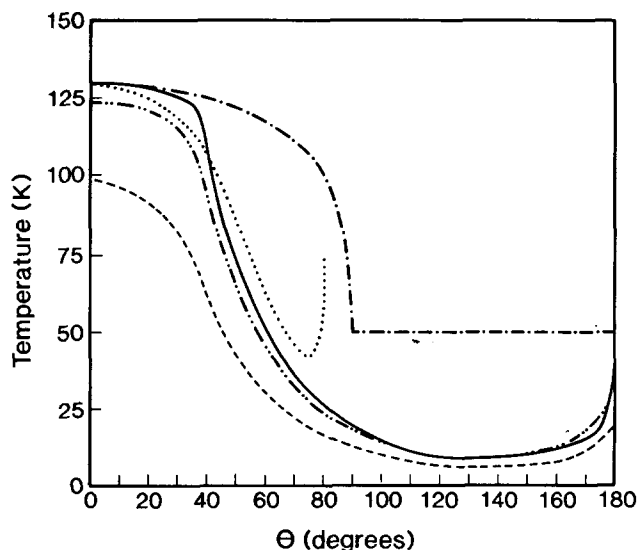


FIG. 3. Atmospheric temperature in the numerical model at $z = 0.4$, 2, and 10 km (solid, dash-double dot, dash) and in the IN85 model (dotted) versus θ for the sublimation atmosphere with $\varepsilon = 0$. The assumed surface temperature $T_s(\theta)$ (dash-dot) is shown for comparison. The atmospheric temperature for the IN85 model is constant over the 10-km thickness of the model atmosphere. The sublimation region is $\theta \leq 37^\circ$.

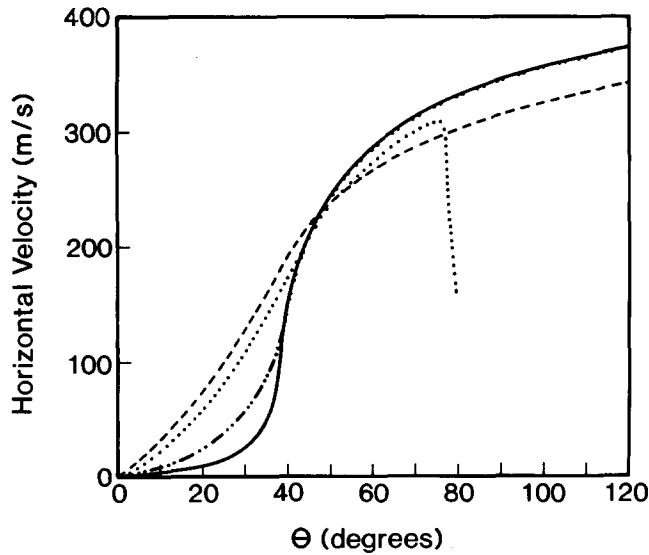


FIG. 4. Horizontal wind velocity as a function of θ for the sublimation atmosphere with $\varepsilon = 0$. Results are shown for the numerical model at $z = 0.4, 2,$ and 10 km altitude (solid, dash-double dot, dash) and for the IN85 model (dotted). The horizontal velocity in the IN85 model is assumed constant over the model atmospheric thickness of 10 km.

A further cooling by about 25 K occurs between $z = 2$ km and $z = 10$ km in the numerical model at $\theta = 0^\circ$. The atmospheric temperature at $\theta = 0^\circ$ in the IN85 model is fixed at the surface temperature of 130 K. The atmospheric temperatures in both models decrease with horizontal distance from the subsolar point because of expansion. The differences in model temperatures can be attributed in part to the neglect of expansion at $\theta = 0^\circ$ in the IN85 model. The upturn in temperature in the IN85 model at $\theta = 76^\circ$ is due to surface friction which has not been included in our numerical model. Temperatures in the numerical model are shown for $\theta > 80^\circ$ even though the continuum approach is not rigorously valid so far from the subsolar point.

Figure 4 shows the dependence on θ of the horizontal wind velocity for the numerical model at $z = 0.4, 2,$ and 10 km and for the IN85 model; horizontal velocity in the IN85 model is height averaged and so does not vary with altitude. The horizontal velocities in the IN85 model and in the numerical model (for $z = 10$ km) are in satisfactory agreement for θ less than about 75° . The sharp decrease in wind velocity for θ greater than about 75° in the IN85 model is due to surface friction. In the numerical model, horizontal wind speeds generally increase with altitude over the sublimation region but decrease with height between 2 and 10 km over the condensation region. Horizontal wind speeds in the numerical model are shown for θ as large as 120° in Fig. 4 despite the breakdown in the continuum theory for $\theta > 80^\circ$.

The structure of the sublimation atmosphere with altitude is illustrated in Fig. 5 which shows meridional cross sections of isobars, isopycnals, and isotherms. The pressure and density contours show the strong thinning of the atmosphere and the isotherms show the strong cooling of the atmosphere with altitude and distance from the subsolar point. The atmospheric structure is significantly two-dimensional, i.e., height variations are substantial even in the subsolar region.

In summary, the results of the numerical model agree quite well with those of the IN85 model. One of the main differences between the models is the atmospheric temperature along the subsolar axis. In the IN85 model this temperature is assumed equal to the surface temperature 130 K. In our numerical model this assumption is relaxed to allow for the expansion and cooling of the atmosphere along the subsolar axis.

6.2. Effects of Infrared Radiative Heat Transfer

The numerical model of the sublimation atmosphere has been used to estimate the potential significance of radiative heat transfer by considering several nonzero values of emissivity. The results for $\varepsilon = 10^{-7}$ and 10^{-6} are indistinguishable from those for $\varepsilon = 0$, but radiative effects become important in the condensation region for $\varepsilon = 10^{-5}$. Radiative transfer between the atmosphere and the relatively hot surface leads to higher near surface atmospheric temperature, pressure, and horizontal wind speed compared with the $\varepsilon = 0$ case for $\theta > 40^\circ$. For

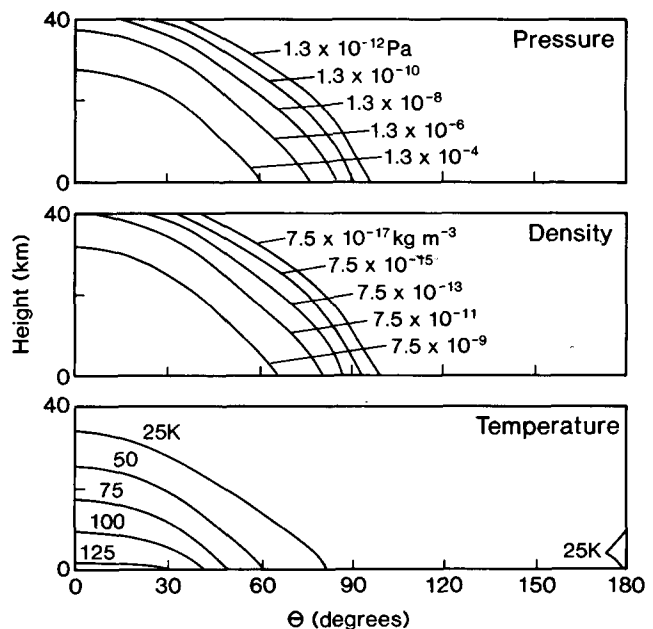


FIG. 5. Isobars, isopycnals, and isotherms in a meridional cross section of the sublimation atmosphere model with zero emissivity.

example, at an altitude of 0.4 km and $\theta = 80^\circ$, the model atmosphere with $\varepsilon = 10^{-5}$ is nearly 25 K hotter and has wind speeds nearly 100 m sec⁻¹ faster than the model atmosphere with $\varepsilon = 0$.

Given the crudeness of our radiative model, it is only possible to conclude that radiative transfer is of possible importance in Io's atmosphere. We have already noted that $\varepsilon = 10^{-5}$ is consistent with Voyager IRIS observations of SO₂ emissions in the Loki region, but it may be too high for regions of low atmospheric density such as the condensation region. Accordingly, the effects of radiative transfer may be more significant in the volcanically derived Io atmosphere, wherein densities near the source region may be relatively high. Our calculations certainly indicate that the effects of radiative heat transfer should be treated more completely in future dynamical models of Io's atmosphere.

6.3. Surface Condensation

It is known that sublimation removes mass from the equator and deposits it at higher latitudes [IN85]. Condensation depletes the atmosphere and negligible deposition takes place beyond $\theta = 80^\circ$. A sublimation atmosphere should produce a band pattern of surface condensation deposits away from the equator. The simplified model of IN85 provided quantitative estimates of condensation rates as a function of angular distance from the subsolar axis; their Table II shows diurnally averaged rates of deposition in 15° bands of latitude. Our numerical two-dimensional model also provides the rates of mass removal and deposition as functions of θ from which we have calculated the integrated surface deposition and found that bands are formed. Because the area of a circumferential band of constant $\delta\theta$ increases with distance from the subsolar point, the mass removed from a narrow sublimation band near the equator spreads over a larger surface area at large θ (if $\theta < 90^\circ$). To calculate the rate at which mass is removed or deposited per unit surface area, we use (5) and the numerical results at time $t = 3 \times 10^4$ sec when a quasi-steady state is established. Figure 6a shows the rates of sublimation and deposition vs θ for the $\varepsilon = 10^{-5}$ case.

Figure 6b illustrates the considerations that enter into determining if there is net condensation over one rotation period at a given Iographic latitude. Three latitude bands are shown in the figure, in each of which it is necessary to evaluate how much mass is removed or deposited per Io rotation. Beyond $\theta = 80^\circ$, it is assumed that neither condensation nor sublimation occurs. In band (a), only condensation occurs, while in band (b), condensation dominates but some sublimation also occurs. In band (c) sublimation dominates. The product of the condensation rate (Fig. 6a) and the surface area for each computational

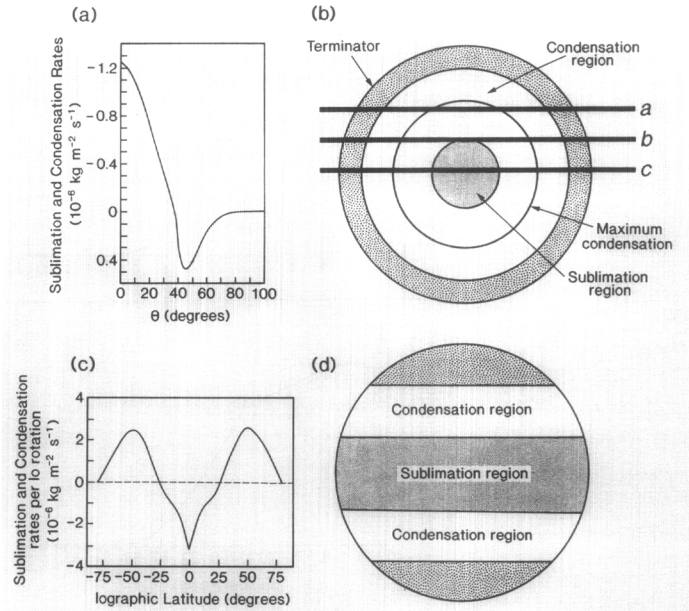


FIG. 6. (a) Sublimation (negative) and condensation (positive) rates vs θ in the numerical model of the sublimation atmosphere with $\varepsilon = 10^{-5}$. (b) Regions of sublimation and condensation relative to the subsolar point. Three latitude bands illustrate the considerations in determining net condensation and sublimation rates at a given Iographic latitude. (c) Average sublimation (negative) and condensation (positive) rates over one Io rotation period as a function of Iographic latitude. (d) Bands of condensation and sublimation.

cell (5° of Io latitude and 5° of Io longitude) along a latitude band must be summed and then divided by the total area of the band to determine the net mass deposition rate per unit surface area per Io rotation period at that latitude. The result, shown in Figs. 6c and 6d, is sublimation in a $\pm 27^\circ$ latitude band and condensation bands poleward of $\pm 27^\circ$ latitude with condensation rate maxima at $\pm 50^\circ$ latitude. There is negligible mass deposition poleward of $\pm 75^\circ$ latitude, consistent with the Voyager observation of the absence of bright polar caps on Io. Because surface temperature decays with distance from the subsolar point and surface vapor pressure depends exponentially on the inverse absolute surface temperature, removal of mass due to sublimation takes place only in a narrow band centered at the equator.

7. VOLCANIC ATMOSPHERES

In contrast to a sublimation atmosphere which is centered at the subsolar point, a volcanic atmosphere can be centered at any position on Io. Here we describe simulations of atmospheres generated by a Pele-type volcanic eruption; one case is centered at the subsolar point with the surface temperature given by $T_s(\theta)$ in Eq. (7) (the dayside volcanic atmosphere) and another case is cen-

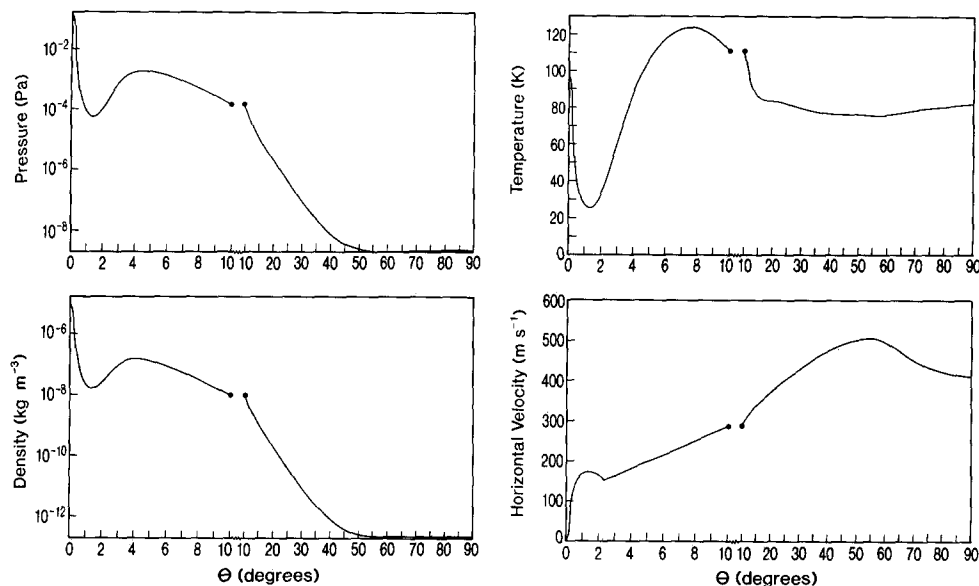


FIG. 7. Near surface ($z = 2.5$ km) pressure, density, temperature, and horizontal velocity for a volcanic night side atmosphere with a source rate of 10^6 kg/sec, surface temperature 90 K, and surface sticking coefficient $\alpha = 1$ plotted as a function of θ the angular distance from the vent. There is a change in scale along the θ axis at about $\theta = 10^\circ$.

tered on a surface with a uniform temperature of 90 K (the nightside volcanic atmosphere). The choice of a surface temperature of 90 K for the nightside is based on observations and a thermal inertia model (Johnson and Matson 1989). The source rate is 10^6 kg/sec, consistent with resurfacing arguments (Johnson *et al.* 1979). The temperature for the volcanic gas as it exits the vent is chosen to be $T = 100$ K, consistent with volcanic eruption studies for Io by Kieffer (1982). In order to facilitate interpretation of the atmosphere produced by a volcano in the presence of dayside sublimation, we first treat the nightside case in which only the volcano contributes significantly. We use an atmospheric emissivity of $\varepsilon = 10^{-5}$ as discussed previously.

7.1. Nightside Volcanic Atmosphere

Figure 7 shows the near surface ($z = 2.5$ km) pressure, density, temperature, and horizontal velocity for the nightside volcanic atmosphere as a function of angular distance θ from the volcanic center. The sudden expansion produces drops in pressure and density of about 3 orders of magnitude within about 2° of the vent. Temperature drops by about 75 K and horizontal wind speeds increase to about 180 m sec^{-1} in the expansion. The increases in pressure and density between about 2° and 4° from the vent are due to a shock that deflects the flow parallel to Io's surface. The shock decelerates the gas and heats it to about 124 K, effectively converting initial kinetic energy of the gas into atmospheric thermal energy. The occurrence of this shock is a major difference be-

tween the volcanic and the sublimation atmospheres. After passing through the shock, further expansion cools the gas to about 80 K and accelerates it to speeds in excess of 500 m sec^{-1} . Surface condensation, which occurs between about $\theta = 2^\circ$ and 56° , localizes the atmosphere to the plume and its immediate vicinity, accounting for the nearly constant and very low values of pressure and density beyond 50° from the vent. Loss of momentum to the surface as a consequence of condensation limits the wind speeds far from the vent. The near surface horizontal flow is supersonic beyond about $\theta = 0.2^\circ$.

Meridional cross sections of isobars, isopycnals, isotherms, and velocity vectors shown in Fig. 8 highlight the location and orientation of the shock which extends from about $\theta = 3^\circ$ near the surface to about $\theta = 25^\circ$ at an altitude $z = 200$ km, thereby making an angle of about 20° with the horizontal. Winds are strongly vertically upward directly above the vent and strongly vertically downward in close proximity to the vent. The downward motions are deflected by the shock to give a nearly horizontal flow beyond the shock region. Constant pressure and density contours are inclined to the surface in close proximity to the vent while they are approximately horizontal at distances from the vent beyond the shock. The atmosphere is strongly heated by the shock as can be seen by the heavy concentration of isotherms in the shock region. The shock is the major feature of the nightside volcanic atmosphere. Some of the detailed structure in the isotherm plot, especially at high altitudes and far from the vent where the densities are very small, may not be physi-

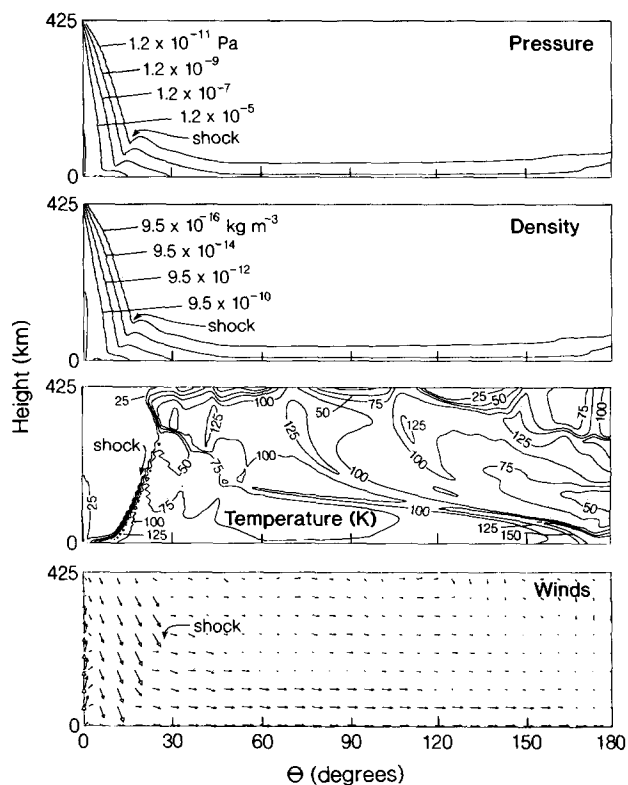


FIG. 8. Isobars, isopycnals, isotherms, and wind velocity vectors in a meridional plane for the nightside volcanic atmosphere corresponding to Fig. 7. Wind speeds are proportional to the lengths of the vectors. The major feature illustrated in these cross sections is the near-vent shock that is inclined to the surface and turns the falling gas parallel to the horizontal.

cally realistic. The region of rigorous validity of the fluid model extends from the vent to about $\theta = 23^\circ$ or to about 800 km from the vent.

7.2. Dayside Volcanic Atmosphere

For the dayside volcanic atmosphere simulation we located the vent at the subsolar point and used the same parameter values as in the nightside simulation except for the surface temperature which was given by Eq. (7). This choice of surface temperature allows a direct comparison of the results with those of a sublimation atmosphere and thus we can infer the effects of a volcanic eruption on the dayside atmosphere. Sublimation and condensation are of course also included in the model.

Figure 9 shows the near surface ($z = 2.5$ km) pressure, density, temperature, and horizontal velocity as a function of angular distance θ from the volcanic vent or subsolar point. Figure 10 shows the atmospheric structure and winds in meridional cross section. The major feature of the dayside volcanic atmosphere is the shock, which is clearly delineated by the abrupt change in slope of the

isobars and isopycnals near the vent, the sudden change in direction of the winds, and the crowding of the isotherms (Fig. 10). Sublimation, which occurs only within about 10° of the subsolar point, "lifts" the shock above the surface (Fig. 10). The volcanic gas does not fall to a cold surface, as in the case of the nightside model, but falls instead onto an obstacle above the surface, the sublimation atmosphere. The shock heats the atmosphere to temperatures above 150 K; the gas subsequently undergoes a general cooling due to expansion (Fig. 9). The expansion beyond the shock accelerates the atmosphere to generally larger horizontal velocities than those in the purely sublimation atmosphere. Figures 9 and 10 also show details of the sudden expansion at the vent, before the gas encounters the shock. The signature of this expansion includes rapid and dramatic decreases in pressure, density, and temperature with both altitude and distance from the vent.

The dayside and nightside volcanic atmospheres are very different in several important respects. Within 25° of the vent or subsolar point, horizontal velocities are higher and atmospheric pressures and densities are lower in the nightside volcanic atmosphere as a consequence of enhanced surface condensation due to the lower surface temperatures near the volcanic source. The enhanced rate of removal of mass in the nightside model produces larger pressure gradients that drive the flow to higher horizontal velocities than in the dayside model before the atmosphere thins out.

Comparison of Figs. 5 and 10 shows that the atmospheric component produced by surface frost sublimation is important at low altitudes, whereas the volcanic component determines the main features of the atmosphere at high altitudes, i.e., above about 10 km, and at the vent at all altitudes. The pressures and densities in the dayside volcanic atmosphere above the vent are much larger than they are in the sublimation atmosphere above the subsolar point at all altitudes, suggesting that the volcanic component dominates the combined dayside atmosphere above the vent. Similarly large pressure and density contrasts occur far from the vent, particularly at high altitudes, implying that the most important contributor to the upper atmosphere is the volcanic source. The range of validity of the fluid dynamic model for the dayside volcanic atmosphere is $\sim 90^\circ$ compared to $\sim 23^\circ$ for the nightside volcanic atmosphere.

7.3. Energy Partitioning

The large horizontal pressure gradients generated by volcanic emissions produce horizontal flow sufficient to establish an extended localized atmosphere on the dayside. On the nightside, there is also substantial horizontal flow away from the plume region. Volcanic atmospheres

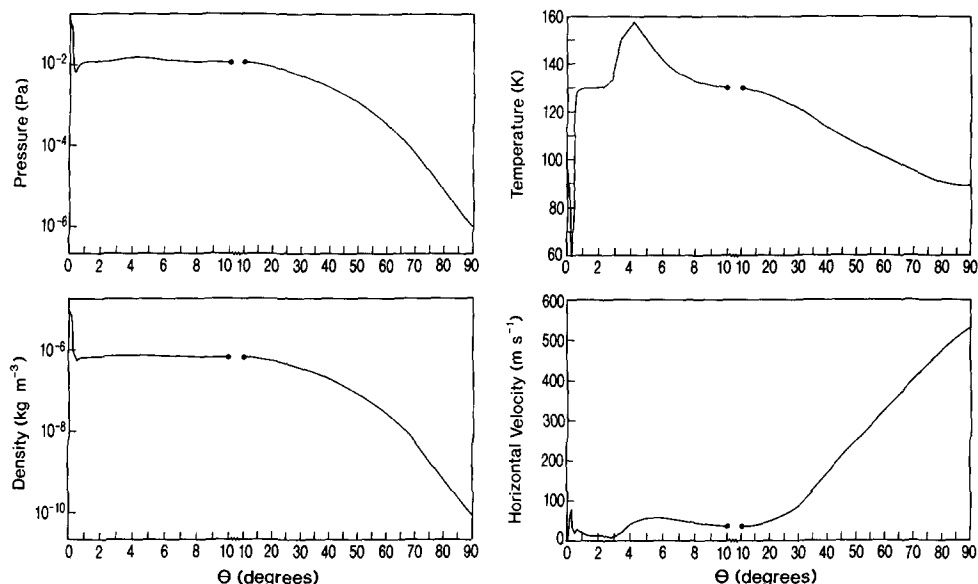


FIG. 9. Similar to Fig. 7, but for the dayside volcanic atmosphere model.

are established on a time scale of several hours (i.e., 3 to 4 hr) after the onset of eruption. In the process of formation of the atmosphere, flow energy is converted into thermal energy which is lost to space by radiation. The rate of kinetic energy input into the atmosphere at the volcanic vent is 5×10^{11} W, while the rate of thermal energy input is 2×10^{10} W; thermal energy is only 4% of the total kinetic energy at the vent exit. However, as the plume gas falls back toward the surface after expanding and going through the shock, the typical flow velocity becomes ~ 0.6 km/sec. Thus $\sim 64\%$ of the initial kinetic energy per unit mass is converted to thermal energy. The redistribution of thermal energy is nonuniform. In the dayside atmosphere, the temperature reaches 150 K in the shock region. Since the main loss of thermal energy takes place via radiation, the shock region emits 10 times more energy per unit area than other parts of the atmosphere. The power emitted in the shock region in the dayside atmosphere is $\sim 2.4 \times 10^{10}$ W, or 5% of the total power input; the surface area of the shock region represents only 0.25 of the total surface area of the atmosphere.

7.4. Horizontal and Vertical Flow Velocities

To compare the results of our volcanic atmosphere simulations with observations, it is pertinent to consider the studies of Lee and Thomas (1980). These authors examined Voyager images of the Pele region and found evidence that material deposits from vents surrounding the Pele volcano were oriented radially away from the vent. They proposed that a near surface horizontal velocity of 130 m/sec is required to transport the micrometer-sized

particles which form the observed tracings at 700 km from the Pele vent. Their inference of 130 m/sec flow velocity was based on an assumed near surface atmospheric pressure of 10^{-2} Pa (consistent with observations of the Loki plume) which at $T = 130$ K corresponds to $\rho = 10^{-7}$ kg/m³ implying a momentum flux of 1.7×10^{-3} kg/m/sec². In our simulation of a volcanic atmosphere with a surface sticking coefficient of 1 we find local mass densities at 700 km from the vent of 5.0×10^{-7} kg/m³ for the dayside and 9.4×10^{-11} kg/m³ for the nightside and near surface horizontal velocities at 700 km from the vent of 60 m/sec for the dayside and 386 m/sec for the nightside. The momentum flux is thus 1.8×10^{-3} kg/m/sec² for the dayside and 2.8×10^{-5} kg/m/sec² for the nightside at 700 km from the vent.

The momentum flux required to transport the particles observed by Lee and Thomas (1980) is thus about the same as the momentum flux in the modeled dayside subsolar volcanic atmosphere at ~ 700 km from the source and larger than the momentum flux in the modeled nightside case by a factor of 100. The observations were made on the dayside but the volcano was not located just at the subsolar point. Since momentum flux decreases with distance from the subsolar point, the dayside volcano simulation provides only an upper limit to the observed flux.

The Voyager 1 observations of a high density envelope of fine particles at the top of the Pele plume (Collins 1981) cannot be explained by ballistic plume models. However, in our gas dynamic model we find that the upward velocity of the gas is 500 m/sec at 300 km (the observed maximum altitude of the Pele plume) and the density at this altitude

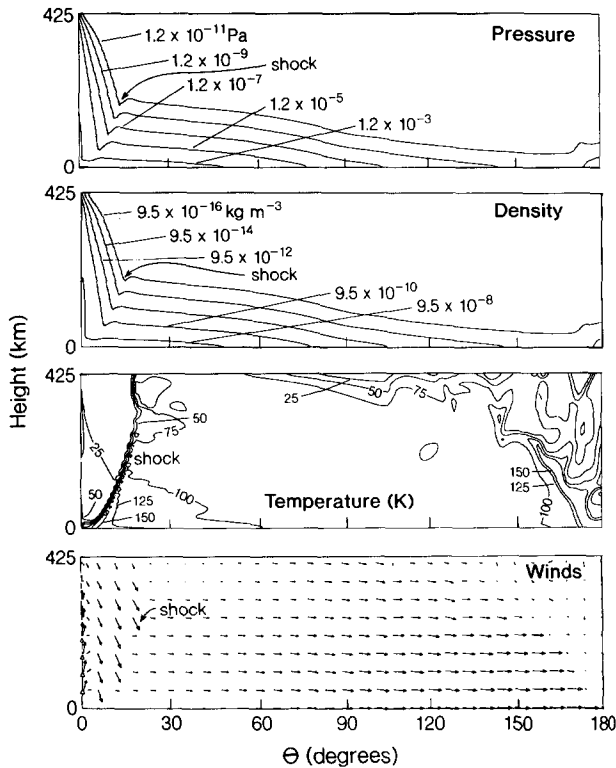


FIG. 10. Isobars, isopycnals, isotherms, and wind velocity vectors in a meridional plane for the dayside volcanic atmosphere corresponding to Fig. 9. Wind speeds are proportional to the lengths of the vectors. A near vent shock that deflects flow parallel to the surface is lifted off the surface by the component of the atmosphere due to sublimation.

is $2.7 \times 10^{-8} \text{ kg/m}^3$. These velocities and densities can produce a momentum flux sufficient to lift and suspend fine particles against the pull of gravity, thus forming the observed high density particulate envelope.

7.5. Surface Condensation, SO_2 Snow, and Ring Deposits for the Nightside Case

Surface condensation is an efficient sink of atmospheric SO_2 especially at low values of surface temperature. Removal of SO_2 gas from the atmosphere by surface condensation allows for the possibility of establishing a quasi-steady atmospheric structure during a prolonged volcanic eruption. Loss of neutrals to the hot torus via sputtering by corotating ions (Moreno *et al.* 1985), on the other hand, represents less than 1% of the source rate, unimportant for the atmosphere despite its importance as a source of magnetospheric plasma.

Pressure gradients near the plume region are enhanced when condensation is important and this leads to an increase in horizontal surface velocities. The higher the condensation rate, the greater the horizontal velocity of the volcanic wind flowing radially away from the plume.

Another consequence of surface condensation is thinning out of the atmosphere as a function of horizontal distance from the plume; the plume region has the characteristic high densities and pressures of a thick atmosphere, while the region far away from the plume has the properties of a thin atmosphere.

Surface condensation of the volcanic gas concentrates deposits in the form of a ring. For both the dayside and the nightside volcanoes, condensation is enhanced in the region near $\theta = 8^\circ$. The condensation deposits are localized on a ring 100 km wide centered at about 250 km from the vent for the nightside volcanic atmosphere and on a ring of similar width but centered at ~ 150 km from the vent for the dayside volcanic atmosphere.

The ratio of ring diameter to plume diameter in the nightside volcanic atmosphere model is $\sim \frac{1}{2}$. The dimensions and locations of the observed ring deposits on Io (Strom *et al.* 1979) are similar to those of the rings in the nightside volcano model. Ballistic trajectory models (Cook *et al.* 1979), on the other hand, predict the location of the rings at the edges of the plumes. The maximum depth of condensed deposits that form the ring, for 1 year of continuous eruption in the nightside model, is ~ 2 cm. Nightside deposits are thicker than dayside deposits because the condensation rate is greater at the surface intersection of the shock in the nightside volcanic atmosphere model than it is at the surface intersection of the shock in the dayside volcanic atmosphere model.

The nightside volcanic atmosphere model predicts the occurrence of snow in the vicinity of the vent. It is well known from studies of snow crystals on earth that volcanic ash and dust particles serve as condensation nuclei and indeed are found at the centers of most snow crystals. Thus, the submicrometer-sized particles (0.01 to $0.1 \mu\text{m}$) of Io's plumes (Collins 1981) should serve as condensation nuclei for SO_2 snow. The region of snow in Io's volcanic atmosphere is the region wherein the atmospheric pressure is greater than the vapor pressure at the surface of a seed particle. The snow region in the nightside volcanic atmosphere model is delineated in Fig. 11, which shows contours of constant $\log_{10}[p - p_v]$, a quantity proportional to the rate of snow formation, as a function of altitude above the vent and angular distance from the vent θ . These calculations were carried out under the assumption that the seed particles have the initial exit temperature of 100 K, i.e., the particles do not reach thermal equilibrium with the atmospheric gas. In this case, the atmospheric pressure is several orders of magnitude greater than the vapor pressure at the surface of the particle.

If the seed particles were to attain thermal equilibrium with the atmosphere, then their temperatures would be less than 100 K in the region around the vent and the vapor pressure at the surface of the particles would be

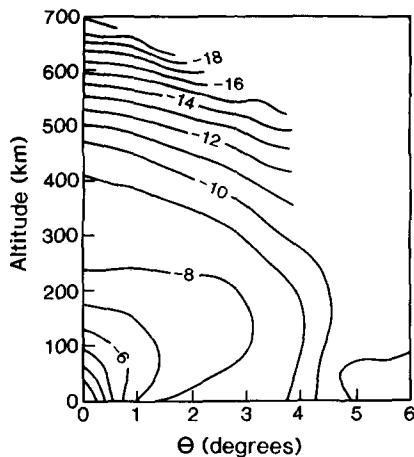


FIG. 11. Region of possible SO_2 snow formation above the vent in the nightside volcanic atmosphere. The contours are curves of constant $\log_{10}[p - p_v]$ in Pa, which is proportional to the rate of snow formation in Io's atmosphere. Snow formation proceeds most rapidly in a region within 240 km directly above the vent. The temperature of the seed particles in this calculation is assumed to be 100 K while the surface temperature is 90 K.

smaller than p_v at $T = 100$ K. In this circumstance, the snow formation rate would be enhanced and the region of snow formation would increase. Thus, Fig. 11 underestimates the region of snow formation. According to the figure, snow formation proceeds most rapidly in a region within ~ 240 km directly above the vent and within 3° (~ 100 km) around the vent.

7.6. The Location of the Exobase

Figure 12 shows the location of the exobase for the sublimation, dayside, and nightside volcanic atmospheres. We calculate the exobase by finding the altitude at which the mean free path for an SO_2 molecule equals the local scale height. This is done by iteration, starting at the top of the atmosphere. The sublimation atmosphere has an exobase located at 55 km above the subsolar point and at the surface near $\theta = 80^\circ$. For the dayside volcanic atmosphere, the exobase is at 550 km above the vent and at the surface near $\theta = 85^\circ$. For the nightside atmosphere, the exobase is located at 400 km above the vent and reaches the surface near $\theta = 23^\circ$.

If the magnetospheric plasma were not perturbed as it approached Io, it would sputter atmospheric neutrals wherever the exobase is above the surface. Dayside atmospheres would then dominate as sources of magnetospheric neutrals, with the dayside volcanic atmosphere serving as the most effective source, because its exobase is the most extended. However, the plasma flow is perturbed as it approaches Io and streamlines tend to align with the surface (Linker *et al.* 1988). In such a flow, the protruding exosphere above both day and nightside

volcanoes may intercept a disproportionately large part of the incident plasma flow and the contributions to sputtering may become correspondingly more important. Possibly, such effects could produce jets of sputtered neutrals localized near volcanic vents. This may explain some of the sodium jets observed by Schneider (1987). In any event, it is likely that these effects increase the importance of the regions close to volcanoes as sources of magnetospheric neutrals.

7.7. The Problem of Oxygen Abundance in the Exosphere

Our model specifies an O/S ratio of 2 : 1 in the exosphere for pure SO_2 eruptions. The specification is based on consideration of the following:

- The time scale for the formation of a quasi-steady state atmosphere is 3 to 4 hr after the onset of eruption.
- Io's upper atmosphere is dominated by the volcanic source.
- The volcanic vapors are exposed to corotating sputtering ions within ~ 1 hr after emerging from the volcano.
- The molecules which are not removed by sputtering after they emerge from the vent are removed from the atmosphere in ~ 4 hr by surface condensation.
- The time scale for dissociation of SO_2 molecules under solar ultraviolet radiation is 23 hr and diffusive transport over one scale height requires several days.

According to the above, neutral molecules reach the

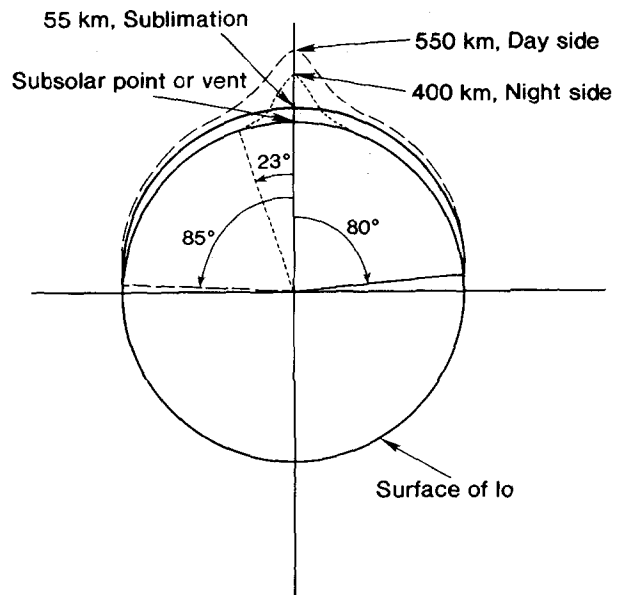


FIG. 12. Location of the exobase for dayside, nightside, and sublimation atmospheres. These produce three different modes of sputtering and source rates to the torus. The dayside volcanic atmosphere may produce localized jets of sputtered neutrals associated with its highest region.

exosphere and can be removed by sputtering to the Io torus before they have sufficient time to dissociate. Also, from the small replenishment and circulation times relative to the molecular dissociation time, we infer that neutral atoms, in contrast to neutral molecules, represent a small fraction of the population of the exosphere. Accordingly, the exospheric source of neutrals for the Io torus must have the composition of the volcanic source itself, i.e., a molecular gas containing one S atom for each pair of O atoms if the volcanic gases are predominantly SO₂. This result is consistent with the cold torus model of Barbosa and Moreno (1987) which requires the presence of a neutral SO₂ cloud in the cold torus region. Other constituents of the source, including sodium and perhaps O₂, are transported to the exosphere in the volcanic models and their presence in the exosphere will affect the composition of the Io plasma torus.

7.8. Post-eclipse Brightening

For about 2.3 hr in each rotational period around Jupiter, Io is in Jupiter's shadow. Binder and Cruikshank (1964) found that in each emergence from Jupiter's shadow the visual brightness of Io was 10 to 15% greater than its brightness in pre-eclipse. The surface of Io cools from 130 K at the subsolar point to about 90 K during the eclipse. The time scale for the surface to reach 130 K again is of order 10³ sec. The observed time scale for the disappearance of the post-eclipse brightening is 900 sec (Binder and Cruikshank 1964). Thus, Binder and Cruikshank (1964) and Sinton (1973) suggested that post-eclipse brightening indicated that Io had an atmosphere and that the brightening was caused by enhanced surface condensation of its constituent gases. However, subsequent observations (Veverka *et al.* 1981) have shown that this phenomenon has not repeated in a periodic way (every ~42 hr) as would be expected from a sublimation atmosphere. Post-eclipse brightening is observed to be sporadic. The Voyager spacecraft observed three eclipse reappearances and there were no increases in brightness at the 10% level (Veverka *et al.* 1981).

We suggest that the sporadic character of post-eclipse brightening is the result of enhanced volcanic eruptions. Since volcanic eruptions are irregular in time, they could produce sporadic brightening. It would thus be useful to search for correlations between post-eclipse brightenings and bursts in the infrared as a test of this idea.

8. COMPARISON OF THE SUBLIMATION AND THE NIGHTSIDE AND DAYSIDE VOLCANIC ATMOSPHERES

There are important qualitative and quantitative differences between volcanic and sublimation atmospheres, as well as between dayside and nightside volcanic atmospheres. The principal difference between the sublimation and the volcanic atmosphere is the absence of a shock in

the sublimation atmosphere. Both the nightside and the dayside volcanic atmospheres develop shocks. In the nightside atmosphere, the shock is closer to the surface than in the dayside volcanic atmosphere. Shocks produce high atmospheric temperatures. The highest atmospheric temperature is found in the shock region of the dayside volcanic model.

The sublimation atmosphere is less extended than the dayside volcanic atmosphere. Both dayside volcanic and sublimation atmospheres are more extended than the nightside volcanic atmosphere formed by a single volcanic eruption. However, multiple volcanic eruptions on the nightside may produce an atmosphere with extension comparable to that of the dayside.

In summary, volcanic atmospheres are on the average warmer than sublimation atmospheres. Volcanic dayside atmospheres have higher horizontal velocities and can extend further than sublimation atmospheres. The highest atmospheric pressures on Io are found in or near volcanic vents and plumes (pressure is an order of magnitude higher than in the sublimation atmosphere).

On the nightside, the atmosphere is completely controlled by volcanic eruptions. We expect that most of the neutrals injected into Jupiter's magnetosphere, which come from the upper atmosphere, are of volcanic origin, but they represent only a small fraction of the source gases. The sublimation neutrals as well as most of the volcanic neutrals are lost to the planetary surface via condensation.

The comparison between the dayside volcanic atmosphere and the sublimation atmosphere provided by Figs. 5 and 10 shows that pressure and density are larger in the dayside volcanic atmosphere than in the sublimation atmosphere particularly above the vent and at high altitudes far from the vent. The volcanic component of the dayside volcanic-sublimation atmosphere dominates above the vent and at high altitudes. A further comparison of the three atmospheres using Figs. 5, 8, and 10 shows that both volcanic atmospheres are warmer than the sublimation atmosphere away from the center of expansion, but above the vent the volcanic atmospheres are colder than the sublimation atmosphere. Both volcanic atmospheres have similar properties above the vent, but away from the vent the nightside volcanic atmosphere is colder and more tenuous than the dayside volcanic atmosphere.

9. IO'S SUBLIMATION H₂S ATMOSPHERE

Recent ground-based observations of Io (Nash and Howell 1989) show an infrared band at 3.915 (±0.015) μm. This band is attributed to reflectance from H₂S frost deposits on the surface of Io. Nash and Howell (1989) also point out that H₂S is widespread on Io's surface, that it may be condensed with SO₂, and that it is temporally variable.

An independent study by Matson and Johnson (1988) also shows that H_2S is present on Io's surface and suggests that it may be an important component in Io's atmosphere. Both groups of authors point out that the observed (Minton 1973) dark polar caps of Io may be due to H_2S deposits. Indeed, laboratory experiments (Lebofsky and Fegley 1976) show that H_2S darkens when irradiated by UV light. Matson and Johnson (1988) have proposed that the atmosphere of Io may contain substantial amounts of H_2S , and that given its high vapor pressure compared to SO_2 , it may meet the requirements of near surface atmospheric pressure inferred from the Pioneer 10 radio occultation experiment (Kliore *et al.* 1975). At the present time there are no complete gas dynamic simulations of an H_2S atmosphere that would allow us to understand its structural and dynamic properties and explain observational constraints. The analysis of Matson and Johnson (1988) is based on a hydrostatic model of an H_2S atmosphere; however, we know from our studies of Io's SO_2 atmosphere that an H_2S atmosphere would be a dynamic one.

We have applied the gas dynamic model developed for the SO_2 sublimation atmosphere to simulate a sublimation atmosphere of H_2S . The only modifications to the SO_2 sublimation model necessitated by considerations of H_2S are the replacement of M_{SO_2} by $M_{\text{H}_2\text{S}}$ in Eqs. (4) and (5) and the use of the H_2S vapor pressure p_v in Eq. (5). The values of A and B for the vapor pressure of H_2S in Eq. (6) are $A = 2.55 \times 10^8$ Pa and $B = 2217$ K. In addition, the H_2S mass flux given by Eq. (5) in the sublimation region is reduced by a factor of 100 to account for a really small concentration of H_2S . The pressure at the terminator in this H_2S sublimation model is found to be two orders of magnitude greater than the lower limit set by the Pioneer 10 radio occultation experiment. The H_2S sublimation atmosphere extends to the nightside and the exobase is above the surface up to $\theta = 155^\circ$. These results suggest that H_2S may be an important component of Io's atmosphere and surface and that inclusion of H_2S in a concentration ratio of 1 : 100 (by number of molecules) with respect to SO_2 in Io's surface frost should be able to produce sufficient atmospheric pressure at the terminator to meet the Pioneer 10 radio occultation requirements. This mixing ratio of $\text{H}_2\text{S}/\text{SO}_2$ is well within the upper limit of 0.35 (by number of molecules) established by Voyager IRIS observations (Pearl *et al.* 1979). The validity of this suggestion requires confirmation by calculation of an atmospheric model with an SO_2 - H_2S mixture.

10. SUMMARY AND CONCLUSIONS

Sublimation Atmosphere

Io's dayside atmosphere likely has contributions from both subliming frost deposits and volcanic eruptions. The nightside atmosphere must be volcanic in origin. The satellite's atmosphere is temporally and spatially variable

due to the sporadic occurrence of volcanic eruptions and the concentration of volcanic atmospheres around the vents, especially on the nightside. Io's atmosphere has supersonic winds and shock waves around volcanic plumes. The atmosphere is likely composed largely of SO_2 but other gases such as H_2S are plausibly present.

A sublimation-condensation SO_2 atmosphere has a source located in the region between $\theta = 0^\circ$ and 37° , and a sink located in the region $\theta = 37^\circ$ to 80° . The sublimation SO_2 atmosphere does not extend to the nightside if the surface sticking coefficient $\alpha = 1$. The sublimation atmosphere is a dynamic one with flow occurring at largely horizontal supersonic velocities between the sublimation and the condensation regions. There are no shock waves in the sublimation atmosphere. Cooling by expansion at the subsolar point causes a decrease of the atmospheric temperature with height in the sublimation atmosphere.

The nightside SO_2 atmosphere is only of volcanic origin. It is strongly localized to regions near volcanic plumes due to the low nightside surface temperatures and the strong dependence of surface condensation rate on surface temperature. The nightside SO_2 volcanic atmosphere is enhanced around the center of volcanic activity; the atmosphere is thick in the region of the plume, but it is thin at large distances from the plume. A shock wave turns the falling volcanic gas in the plume away from the surface and the gas flows horizontally away from the plume region at large supersonic speeds.

The dayside SO_2 atmosphere likely consists of both sublimation and volcanic components. A dayside volcanic atmosphere also features an oblique shock to turn falling volcanic gas parallel to the surface. The shock is lifted above the surface by the sublimation component of the dayside atmosphere. The dayside volcanic atmosphere extends farther from the vent and higher than either the nightside volcanic atmosphere or the sublimation atmosphere. However, the dayside volcanic atmosphere with the vent near the subsolar point does not extend beyond the terminator. The near surface momentum flux for a dayside SO_2 volcanic atmosphere is consistent with observations of winds blowing vent emissions at 700 km from the main vent. The highest temperatures in Io's atmosphere will be found in the shock regions of volcanic plume sources.

A volcanically derived Io atmosphere allows the composition of the exosphere to be a function of source composition. The source of the Io torus plasma can be matched to torus composition because of the short time scale of exposure of the volcanic gas to sputtering corotating ions in comparison to the time scales for dissociation and atomic diffusion. A single step mechanism suffices for the removal of sodium from Io to the neutral cloud. A volcanic eruption exposes sodium as well as sulfur dioxide to the corotating plasma on very short time scales (~ 1 hr), provided there is some sodium in the plume vapors. Both

volcanic and sublimation atmospheres allow for a 1:2 ratio of S : O because the removal time scale by condensation in these dynamic atmospheres is short (several hours) compared to the dissociation time scale. The high altitude exobase above volcanic vents on either the dayside or the nightside may serve as an important source of sputtering neutrals because magnetospheric plasma, diverted by its interaction with Io, can readily flow onto regions of protruding atmosphere.

Surface condensation is the most important sink mechanism for volcanic gas in both the nightside and the dayside SO₂ atmospheres. Surface condensation is nonuniform as a function of distance from the vent and for both volcanic atmospheres it produces enhanced deposits in the form of a ring. The model predictions regarding the locations and dimensions of the rings agree with Voyager observations. Surface condensation for an SO₂ sublimation atmosphere produces a band pattern of surface deposits. Removal of surface frost takes place from an equatorial band of $\pm 27^\circ$ Iographic latitude, while deposition takes place from 27° to $\sim 70^\circ$ with a maximum rotation-averaged deposition at $\pm 50^\circ$. There is no observational evidence for a band-pattern of surface condensation on Io.

Although the sublimation atmosphere does not develop a shock in our model with a smooth surface, the supersonic flow could lead to shocks if surface topography is included. Similar effects could also occur in volcanic atmospheres away from the plumes. The same mechanism that produces ring deposits will also produce enhanced deposits around mountains or other topographic obstacles in the path of the volcanic or sublimation supersonic winds. The camera on the Galileo spacecraft has sufficient resolution to observe these features should they occur.

An SO₂-H₂S sublimation atmosphere with a surface frost concentration ratio of H₂S to SO₂ of $\frac{1}{100}$ (by number of molecules) may be able to reproduce the Pioneer 10 radio occultation measurements of pressure at Io's terminator. An H₂S volcanic atmosphere with characteristics (e.g., source rate) similar to those of an SO₂ volcanic atmosphere should extend farther from the vent than the SO₂ atmosphere because H₂S is a less condensible vapor than SO₂.

Radiative effects may be important in determining the behavior of Io's sublimation and volcanic atmospheres in regions where the atmospheres are dense enough for $\epsilon \approx 10^{-5}$. Future models of Io's atmospheric dynamics should incorporate more detailed and rigorous treatments of radiative heat transfer.

APPENDIX A

Radiative Transfer Model

In the present model, our treatment of radiation is highly simplified. We consider only the effects of radiation at infrared wavelengths and all calculated radiative fluxes are assumed to be in the radial direction. The

TABLE I
Band Equivalent Widths and Planck-Weighted Column Absorptivities for SO₂ Gas Path Lengths of 0.1 and 1.0 cm-atm

ν_0 (cm ⁻¹)	Band equivalent width (cm ⁻¹)	Column absorptivity	
		$T = 80$ K	$T = 130$ K
Path length = 0.1 cm-atm			
1151.4	0.43	1.0×10^{-8}	4.9×10^{-6}
517.7	0.43	8.4×10^{-5}	4.4×10^{-4}
1361.8	3.40	3.8×10^{-9}	6.2×10^{-6}
Path length = 1.0 cm-atm			
1151.4	0.73	1.8×10^{-8}	7.5×10^{-6}
517.7	0.73	1.4×10^{-4}	7.5×10^{-4}
1361.8	5.80	6.5×10^{-9}	1.0×10^{-5}

atmosphere is assumed to be composed of purely SO₂ gas which is assumed to be transparent except in the ν_1 , ν_2 , and ν_3 band where the individual bands have strong, nonoverlapping line centers. Each mass element in the atmosphere is cooled by radiating to space and is heated by thermal emission from the surface, which is assumed to be a blackbody at a fixed temperature. The rate of absorption or emission for each element is proportional to its mass.

Pearl *et al.* (1979) have used line calculations to determine the equivalent widths of the three SO₂ infrared bands for comparison with the Voyager IRIS observations. Table I shows these equivalent widths (J. Pearl, personal communication) and calculated Planck-weighted column absorptivities for optical paths of 0.1 and 1.0 cm-atm at temperatures of 80 and 130 K.

The calculations show that at Io temperatures, the infrared absorptivity of the atmosphere is dominated by the ν_2 band at 517.5 cm⁻¹, with typical bolometric column absorptivities of approximately 10^{-4} to 10^{-5} . These column absorptivities are likely to be upper limits due to the breakdown of local thermodynamic equilibrium (LTE). We have made estimates of the expected non-LTE cooling rate in Io's atmosphere by using the formulation of Houghton (1986) and by following Kumar's assumption that the SO₂ collisional deactivation coefficients are the same as for CO₂ (Kumar 1984). The results show that LTE is a good approximation only for number densities greater than approximately 10^{12} , which generally occur in the lowest two scale heights of Io's atmosphere. At higher altitudes, the breakdown of LTE should result in significantly smaller heating and cooling rates.

In the model calculations that include the effects of radiation we vary the Planck-weighted column emissivity of the atmosphere from 0 to 10^{-5} . The value of 10^{-5} is consistent with the Voyager IRIS observations of atmospheric SO₂ emission on Io, but it may be far too high in regions of low atmospheric density. In future models, it would be very desirable to include a more complete radiation code that includes the effects of solar heating, non-LTE infrared cooling, and the radiative effects of atmospheric aerosols.

APPENDIX B

Numerical Method

Equations (1)–(4) were solved using the numerical code CAVEAT developed by Adessio *et al.* (1986) at Los Alamos National Laboratory and modified by one of us (J. Baumgardner) to address the case of the Io atmosphere. CAVEAT is designed to solve a wide class of transient, multimaterial, compressible fluid dynamics problems. It uses a time explicit, conservative finite-volume formulation in which all variables,

including velocities, are cell-centered. The two-dimensional version used here has options for both Cartesian and axisymmetric geometries. The computational mesh consists of logically rectangular blocks of arbitrary quadrilateral cells.

One of the central features of CAVEAT is its use of the Godunov method (Dukowicz 1985). This method involves solving a Riemann problem for each cell face in the mesh to resolve the discontinuity arising from the differing conditions in the cells on the two sides of a given face. The method naturally and automatically handles shock waves, interfaces between different materials, and free surfaces. It yields shock wave solutions that typically are only one to three cells in thickness, and it does so without the need for artificial viscosity or other arbitrary parameters. It has the desirable mathematical properties of monotonicity and correct sense of information flow. The main disadvantage of the method has been the expense of solving the nonlinear Riemann problems, particularly for materials with complex equations of state. This difficulty has been overcome almost completely by a general, noniterative Riemann solver developed by Dukowicz (1985) which requires only two material-dependent parameters that are conveniently obtained for materials with complex equations of state from linear fits to the experimental shock Hugoniot data. For an ideal gas, however, the parameters are given by simple algebraic expressions.

The Godunov method is formulated most naturally in terms of cell-centered variables and a finite volume approach for solving the conservation equations. With the finite volume method, the Eulerian conservation equations [(1)–(3)] are expressed in integral form, using the divergence theorem to recast the volume integrals of the divergence terms as surface integrals. The integration volumes for mass momentum and energy are all identical and correspond simply to the cells in the mesh. The cell-face pressures and velocities obtained as the Riemann problem solutions are utilized in a natural fashion to evaluate the surface integrals over the four faces of each cell. The code is highly vectorized for efficient execution on Cray computers.

CAVEAT has been tested extensively for problems involving shocks in a number of geometries. The comparison of computational results with experimental data as well as with analytical solutions indicates that the code is robust and highly accurate (Sandoval 1986). Application of CAVEAT to the problem of volcanic plumes on Io requires modification of the code to add the gravitational body force term in the momentum equation, to include the proper radiation term in the energy equation, and to account for the condensation and sublimation of SO₂ at the satellite's surface.

ACKNOWLEDGMENTS

This work was partially supported by NASA Grants 7295 and NSG7164 and IGPP LANL Grant 208. Institute of Geophysics and Planetary Physics publication 3044. The authors thank Dr. R. J. Walker and Dr. D. Hunten for many helpful discussions and Dr. A. Ingersoll for identifying points in the initial version of this paper which required revision. M. Moreno acknowledges with thanks access to the Cray computers and the hospitality of Los Alamos National Laboratory.

REFERENCES

- ADESSIO, F. L., D. E. CARROL, J. K. DUKOWICKS, F. H. HARLOW, J. N. JOHNSON, B. A. KASHIW, M. E. MALTRUD, AND H. M. RUPPEL 1986. *Caveat: A Computer Code for Fluid Dynamics Problems with Large Distortion and Internal Slip*. Los Alamos National Laboratory, Internal Publication LA-10613-MS.
- BARBOSA, D. D., AND M. A. MORENO 1987. A comprehensive model of ion diffusion and charge exchange in the cold Io torus. *J. Geophys. Res.* **93**, 823–836.
- BELTON, M. J. S. 1982. An interpretation of the near-ultraviolet absorption spectrum of SO₂: Implications for Venus, Io, and laboratory measurements. *Icarus* **52**, 149–165.
- BINDER, A. B., AND D. P. CRUIKSHANK 1964. Evidence for an atmosphere on Io. *Icarus* **3**, 299–305.
- BRYSON, C. E., V. CAZCARRA, AND L. L. LEVENSON 1974. Condensation coefficient measurements of H₂O, N₂O and CO₂. *J. Vac. Sci. Technol.* **11**, 411–416.
- BUTTERWORTH, P. S., J. CALDWELL, V. MOORE, T. OWEN, A. R. RIVOLO, AND A. L. LANE 1980. An upper limit to the global SO₂ abundance on Io. *Nature* **285**, 308.
- COLLINS, S. A. 1981. Spatial color variations in the volcanic plume at Loki on Io. *J. Geophys. Res.* **86**, 8621–8626.
- COOK, A. F., E. M. SHOEMAKER, AND B. A. SMITH 1979. Dynamics of volcanic plumes on Io. *Nature* **280**, 743–746.
- DUKOWICZ, D. K. 1985. A general non-iterative Riemann solver for Godunov's method. *J. Comp. Phys.* **61**, 119–137.
- HOUGHTON, J. T. 1986. *The Physics of Atmospheres*, Cambridge University Press.
- HUNTEN, D. M. 1985. Blowoff of an atmosphere and possible applications to Io. *Geophys. Res. Lett.* **12**, 271–273.
- INGERSOLL, A. P., M. A. SUMMERS, AND S. G. SCHLIPF 1985. Supersonic meteorology of Io: Sublimation driven flow of SO₂. *Icarus* **64**, 375–390.
- INGERSOLL, A. P. 1989. Io meteorology: How atmospheric pressure is controlled locally by volcanoes and surface frosts. *Icarus* **81**, 298–313.
- JOHNSON, T. V., A. F. COOK, C. SAGAN, AND L. A. SODERBLOM 1979. Volcanic resurfacing rates and implications for volatiles on Io. *Nature* **280**, 746–750.
- JOHNSON, T. V., AND D. L. MATSON 1989. In *Origin and Evolution of Planetary and Satellite Atmospheres* (S. K. Atreya, J. B. Pollack, and M. S. Matthews, Eds.), pp. 666–681. Univ. of Arizona Press, Tucson, Arizona.
- KIEFFER, S. W. 1982. In *Satellites of Jupiter*, (D. Morrison, Ed.), pp. 647–723. Univ. of Arizona Press.
- KLIORE, A., G. FJELDBO, B. L. SEIDEL, D. N. SWEETMAN, T. T. SESPLAUKIS, AND P. M. WOICESHYN 1975. Atmosphere of Io from Pioneer 10 radio occultation measurements. *Icarus* **24**, 407–419.
- KUMAR, S., AND D. M. HUNTEN 1982. In *Satellites of Jupiter* (D. Morrison, Ed.), pp. 782–806. Univ. of Arizona Press, Tucson, Arizona.
- KUMAR, S. 1980. A model of the SO₂ atmosphere and ionosphere of Io. *Geophys. Res. Lett.* **7**, 9–12.
- KUMAR, S. 1984. Sulfur and oxygen escape from Io and a lower limit to atmospheric SO₂ at Voyager 1 encounter. *J. Geophys. Res.* **89**, 7399–7406.
- KUMAR, S. 1985. The SO₂ atmosphere and ionosphere of Io: Ion chemistry, atmospheric escape, and models corresponding to Pioneer 10 radio occultation measurements. *Icarus* **61**, 101–123.
- LEBOFSKY, L. A., AND M. B. FEGLEY 1976. Laboratory reflection spectra for the determination of chemical composition of icy bodies. *Icarus* **28**, pp. 379–387.
- LEE, S. W., AND P. G. THOMAS 1980. Near surface flow of volcanic gases on Io. *Icarus* **44**, 280–290.
- LELLOUCH, E., M. BELTON, I. PATER, S. GULKIS, AND T. ENCRENAZ 1990. Io's atmosphere from microwave detection of SO₂. *Nature* **346**, 639–641.
- LINKER, J. A., M. G. KIVELSON, AND R. J. WALKER 1988. An MHD

- simulation of plasma flow past Io: Alfvén and slow mode perturbations. *Geophys. Res. Lett.* **15**, 1311–1314.
- MATSON, D. L., AND D. B. NASH 1983. Io's atmosphere: Pressure control by regolith cold trapping and surface venting. *J. Geophys. Res.* **88**, 4771–4783.
- MATSON, D. L., AND T. V. JOHNSON 1988. Io's atmosphere: Evidence for H₂S. *EOS Trans. AGU* **69**, 1227.
- MCEWEN, A. S., AND L. A. SODERBLOM 1983. Two classes of volcanic plumes on Io. *Icarus* **58**, 197–226.
- MCEWEN, A. S., T. V. JOHNSON, D. L. MATSON, AND L. A. SODERBLOM 1988. The global distribution, abundance, and stability of SO₂ on Io. *Icarus* **75**, 450–478.
- MINTON, R. B. 1973. The red polar caps of Io. *Commun. Lunar Planet. Lab.* **10**(188), 35–39.
- MORENO, M. A., W. I. NEWMAN, AND M. G. KIVELSON 1985. Ion partitioning in the hot Io torus: The influence of S₂ outgassing. *J. Geophys. Res.* **90**, 12,065–12,072.
- MORENO, M. A., AND D. D. BARBOSA 1986. Mass and energy balance in the cold Io torus. *J. Geophys. Res.* **91**, 8993–8997.
- MORENO, M. A., M. G. KIVELSON, G. SCHUBERT, AND J. BAUMGARDNER 1986. A plume driven atmosphere of Io, *EOS Trans. AGU* **63**, 1062.
- MORENO, M. A., G. SCHUBERT, M. G. KIVELSON, AND J. BAUMGARDNER 1987. In *Abstracts of the International Workshop on Time-Variable Phenomena in the Jovian System*. Flagstaff, Arizona, August 25–27.
- NASH, B., AND R. R. HOWELL 1989. Hydrogen sulfide on Io: Evidence from telescopic laboratory infrared spectra. *Science* **244**, 454–457.
- PEARL, J., R. HANEL, V. KUNDE, W. MAGUIRE, K. FOX, S. GUPTA, C. PONNAMPERUMA, AND F. RAULIN 1979. Identification of gaseous SO₂ and new upper limits of other gases on Io. *Nature* **280**, 755–758.
- SANDEVAL, D. L. 1986. *Caveat Calculations of Shock Interactions*. Los Alamos National Laboratory, Preprint, LA-1100-MS.
- SCHNEIDER, N. M. 1987. Velocity structure of the Io sodium cloud. *Bull. Am. Astron. Soc.* **19**, 854–855.
- SCHNEIDER, N. M., D. M. HUNTEN, W. K. WELLS, AND L. M. TRAFTON 1987. Eclipse measurements of Io's sodium atmosphere, *Science* **238**, 55–58.
- SHEMANSKY, D. E., AND G. R. SMITH 1981. The Voyager 1 EUV spectrum of the Io plasma torus. *J. Geophys. Res.* **86**, 9179–9192.
- SHEMANSKY, D. E. 1987. The ratio of oxygen to sulfur in the Io plasma torus. *J. Geophys. Res.* **92**, 6141–6146.
- SIMONELLI, D. P., AND J. VEVERKA 1986. Phase curves of materials on Io: Interpretation in terms of Hapke's function. *Icarus* **68**, 503–521.
- SINTON, W. M. 1973. Does Io have an ammonia atmosphere? *Icarus* **20**, 284–296.
- SMITH, B. A., AND S. A. SMITH 1972. Upper limits for an atmosphere on Io. *Icarus* **17**, 218–222.
- STROM, R. G., R. J. TERRILE, H. MASURSKY, AND C. HANSEN 1979. Volcanic eruption plumes on Io. *Nature* **280**, 733–736.
- STROM, R. G., AND N. M. SCHNEIDER 1982. In *Satellites of Jupiter* (D. Morrison, Ed.), pp. 598–633. Univ. of Arizona Press, Tucson, Arizona.
- SUMMERS, M. E. 1985. *Theoretical Studies of Io's Atmosphere*. Ph.D. thesis, California Institute of Technology.
- VEVERKA, J., D. SIMONELLI, P. THOMAS, D. MORRISON, AND T. V. JOHNSON 1981. Voyager search for post-eclipse brightening on Io. *Icarus* **47**, 60–74.